Controlled synthesis of starch-based branched polymers

Fan, Yifei

Chapter 5

Highly branched waxy potato starch-based polyelectrolyte: Controlled synthesis and the influence of chain composition on solution rheology

Abstract

In the present work, a series of highly branched random copolymers of acrylamide (AM), sodium 2-acrylamido-2-methyl-1-propanesulfonate (SAMPS) and *N*-isopropylacrylamide (NIPAM) were prepared by using water-soluble waxy potato starch as macroinitiator via aqueous Cu^0-mediated living radical polymerization (Cu^0-mediated LRP) at room temperature. The intake of SAMPS and NIPAM in the copolymers were varied to investigate the influence of chain composition on the aqueous rheological properties of the prepared copolymers. Comparison between different starch-based AM/SAMPS copolymers indicated an optimum SAMPS intake (25 mol%) for the balanced performance of viscosity and salt resistance in high salinity water. A high intake of NIPAM units (e.g. 25 mol%), contrary to what expected, undermines the thickening ability of the copolymers in saline water due to the hydrophobic association. In high salinity solution, thermo-thickening behavior can be observed at low shear rates ($\gamma \leqslant 3\ s^{-1}$) because of the screening effect of salt on the negatively charged SAMPS units. At a higher shear rate, the thermo-thickening behavior disappears due to the disruption of the NIPAM aggregates.

This chapter is based on Yifei Fan, Ranjita K. Bose, and Francesco Picchioni, Highly Branched Waxy Potato Starch-based Polyelectrolyte: Controlled Synthesis and the Influence of Chain Composition on Solution Rheology (2018), to be submitted

5.1. Introduction

Enhanced oil recovery (EOR) is a widely used technique to promote the oil production due to the increasing demand on oil and the relatively large portion (~ 40% of original oil) of unexploited residual oil [1]. Polymer flooding is one common EOR method entailing the use of a polymer as thickener to reduce the mobility difference between water and oil and thus increase the sweep efficiency of water on the porous structure where crude oil is deposited. Partially hydrolyzed polyacrylamide (HPAM) has been widely used in recent decades for polymer flooding because of its low cost [2,3]. However, HPAM tends to hydrolyze and precipitate out in the reservoirs, especially in those with high temperature (up to 130 ˚C) and salinity (up to 200000 ppm, in particular when divalent cations like Ca^{2+} and Mg^{2+} are present) [4-6]. This is detrimental to the performance of polymer flooding and also harmful to the reservoir. In this case, carefully designed polymers, that can withstand the hostile (saline) environment, are needed for sustainable exploration. Another problem in the oilfield exploitation is the management of produced water which is a by-product with a large volume. This kind of water usually contains a variety of organic and inorganic pollutants like hydrocarbons, heavy metals, chemicals during drilling, and in most cases also has high salinity [7]. Reinjection of produced water for EOR is one attractive option for the sake of environment (fragile ecosystems like offshore and Arctic areas) and reservoir protection (the use of a different water source might result in the significant formation of precipitated salts, thus damaging to the reservoir exploration) [8]. The utilization of saline-resistant polymers may be helpful to achieve this purpose.

The salt-resistance of polymers, like many other properties, is also affected by both their composition and structure. For example, a previous study revealed that branched structures can result in higher viscosity and better viscoelastic properties than linear ones [9,10]. In the case of comb-like polymers grafted with a mixture of *N*-isopropylacrylamide (NIPAM) and acrylamide (AM), it has been reported that a random NIPAM distribution in the side chains (as opposed to block copolymers grafted chains) could endow the product with better thermo-thickening behavior and solubility in water for applications like EOR [11]. Based on this, in our previous research, a series of highly branched AM/NIPAM random copolymers (St-g-(PAM-co-PNIPAM)) was synthesized based on waxy potato starch and its highly branched structure composed of 10^5 - 10^6 anhydroglucose units (AGU) (see illustration Figure S5-1) [12-15]. Waxy potato starch-based branched copolymer is supposed to have a relatively stable hydrodynamic volume because of the steric hindrance inherent to its structure. As a matter of fact, St-g-(PAM-co-PNIPAM) with optimized NIPAM intake (e.g. 25 mol%) displayed both thermo-thickening

behavior and stable viscosity profile in different saline solutions [12].

Despite the balanced performance, however, efforts are still needed to improve the solubility (dissolve faster) and viscosity of copolymers under relatively low salinity compared with that of commercial HPAM products. One option is the incorporation of salt-resistant polyelectrolyte segments in the highly branched structure. Poly(2-acrylamido-2-methyl-1-propanesulfonic acid sodium salts) (PAMPS), as an anionic polyelectrolyte bearing negative charges in polymer chains like HPAM, is reported to be more stable at high temperature in saline water [16,17]. Moreover, PAMPS polymers are now also recognized as potential materials for bioengineering [18], forward osmosis [19,20], catalysts support for energy and environment applications [21]. Thus, the synthesis of PAMPS and its copolymers has been an interesting research topic in recent years [22-25].

In the case of grafting PAMPS (co)polymers onto starch, generally, the reaction is carried out in water by free radical polymerization with ceric salts as initiator [23,26]. As reported, by using controlled polymerization, like transition metal (mainly Cu(I)) mediated atom transfer radical polymerization (ATRP), Cu^0-mediated aqueous living radical polymerization (Cu^0-mediated LRP) and reversible addition-fragmentation chain transfer (RAFT), the formation of homopolymer, typical for conventional free radical polymerization, can be avoided and tailor-made properties can be achieved [12,22,23]. This is favorable for the investigation of the influence of chain length and structure on (co)polymer properties. Compared with RAFT, which usually should be carried out above 50 ˚C, and normal ATRP, Cu^0-mediated LRP could be achieved at room temperature or even lower (0 ˚C for example) while maintaining a much higher polymerization rate in aqueous solution [27]. However, reports on the synthesis of PAMPS and its copolymers by Cu^0-mediated LRP are still rare compared with RAFT and "classical" ATRP [24,28-30].

In the present study, 2-acrylamido-2-methyl-1-propanesulfonic acid (AMPS) was neutralized with sodium hydroxide to avoid the influence of low pH on the activity of the catalyst and the controllability of Cu^0-mediated LRP on the synthesis of poly(sodium 2-acrylamido-2-methyl-1-propanesulfonate) (PSAMPS) in water was then verified. Meanwhile, a water-soluble waxy potato starch-based macroinitiator was synthesized homogeneously in *N*,*N*-dimethylacetamide (DMAc)/LiCl solution [31,32]. Based on these, copolymers of sodium 2-acrylamido-2-methyl-1-propanesulfonate (SAMPS), acrylamide (AM) and *N*-isopropylacrylamide (NIPAM) were grafted from the starch backbone by Cu^0-mediated LRP in aqueous phase. The macroinitiator and (co)polymers were characterized by NMR and FT-IR. For the potential applications like EOR, the ratio of the three monomers was varied to study the influence of chain composition

on the rheological properties of (co)polymer solutions and their response to temperature and saline water.

5.2. Experimental section

5.2.1. Materials

Waxy potato starch (> 95% amylopectin) was kindly donated by Avebe (The Netherlands) and dried under vacuum at 60 ˚C for 48 h before use. Lithium chloride was purchased from Sigma-Aldrich and dried under vacuum at 80 ˚C for 24 h before use. Anhydrous *N*,*N*-dimethylacetamide (DMAc) was purchased from Sigma-Aldrich in Sure/Seal™. 2-bromopropionic acid (BpA), 2-bromopropionyl bromide (BpB), formaldehyde solution (37%) and formic acid (> 95%) were purchased from Sigma-Aldrich and used as received. Tris(2-aminoethyl)amine (Tren) was purchased from TCI and used as received. Tris[2-(dimethylamino)ethyl]amine (Me_6Tren) was synthesized following the procedures reported [33]. 2-Acrylamido-2-methyl-1-propanesulfonic acid (AMPS) was purchased from Sigma-Aldrich and neutralized with sodium hydroxide (from Sigma-Aldrich) in Milli-Q solution which was then poured into tenfold acetone to obtain the solid sodium 2-Acrylamido-2-methyl-1-propanesulfonate (SAMPS). Acrylamide (AM) was purchased from Sigma-Aldrich and used as received. *N*-Isopropylacrylamide (NIPAM, stabilized with MEHQ) was purchased from TCI and recrystallized from acetone to remove the inhibitor. Copper powder (< 75 μm) was purchased from Sigma-Aldrich and stored under N_2 atmosphere. Linear partially hydrolyzed polyacrylamide (L-HPAM) with molecular weight around 10 million Dalton and degree of hydrolysis around 30% was obtained by free radical polymerization.

5.2.2. Instruments and analysis

The composition of the synthesized copolymer was determined by Elementar vario MICRO cube CHNS elemental analyzer. For starch-based grafted copolymer without NIPAM intake, samples were taken after Soxhlet extraction as the trace solvent (ethanol) impurities has no influence on the result. For the NIPAM containing copolymers, samples from the Soxhlet extraction were dissolved in Milli-Q water and rotovap was used to remove the trace solvent. The obtained samples were freeze-dried for one day before the test. The ratio of monomer units can be obtained according to the following equation:

$$\gamma(\mathrm{SAMPS}) = \frac{14 \times S\%}{32 \times N\%} \qquad \textbf{5.1}$$

$$\gamma(\mathrm{AM}) = \frac{1}{3} \times \left(6 - \frac{14 \times C\%}{12 \times N\%} + \frac{14 \times S\%}{32 \times N\%} \right) \qquad \textbf{5.2}$$

where γ(SAMPS) and γ(AM) stands for the mole ratio of SAMPS and AM in the copolymer respectively, *C*%, *N*%, and *S*% is the mass ratio of carbon, nitrogen, and sulfur in the copolymer respectively (see Table S5-1).

NMR spectra were recorded on Varian Mercury Plus 400 MHz spectrometer using deuterated solvents purchased from Sigma-Aldrich. Fourier Transform Infrared (FT-IR) spectra were recorded with attenuated total reflection (ATR) accessories on an IRTracer-100 SHIMADZU Fourier Transform Infrared Spectrophotometer and data were processed with LabSolutions IR software. Aqueous gel permeation chromatography (GPC) was conducted on an Agilent 1200 system equipped with a differential refractive index (DRI) detector and Polymer Standard Service (PSS) column set (PSS SUPREMA 100 Å, 1000 Å, 3000 Å). The mobile phase used was 0.05 M $NaNO_3$. Column oven and detector temperatures were regulated to 40 ˚C, flow rate 1 mL/min. Polyethylene oxide standards (ReadyCal, M_p 200 - 1200000) from Fluka were used for calibration. Samples were filtered through a membrane with 0.22 μm pore size before injection. Experimental molar mass and polydispersity index (PDI) values of synthesized polymers were determined by conventional calibration using Agilent GPC/SEC software.

Rheological properties were measured by a HAAKE Mars III (Thermo Scientific) rheometer equipped with a cone-and-plate geometry (diameter 60 mm, angle 2˚). Solution viscosity was measured as a function of shear rate (0.1 to 1750 s^{-1}, T = 20 ˚C), salt concentration (5000 - 100000 ppm of NaCl, T = 20 ˚C, shear rate 10 s^{-1}) and temperature (10 ˚C to 95 ˚C, shear rate 1 s^{-1}, 3 s^{-1} and 10 s^{-1}) respectively.

The intrinsic viscosity was determined according to the Martin equation [34]:

$$\eta_{red} = \frac{\eta_{sp}}{c} = [\eta] e^{\kappa_M c[\eta]} \qquad \textbf{5.3}$$

where η_{red} is the reduced viscosity, η_{sp} is the specific viscosity, c is the polymer concentration, $[\eta]$ is the intrinsic viscosity and k_M is a constant depends on the polymer-solvent system.

The relaxation time (λ) was determined according to the Carreau-Yasuda model [9,35,36]:

$$\frac{\eta-\eta_\infty}{\eta_0-\eta_\infty}=\left[1+\left(\lambda\cdot\gamma\right)^\alpha\right]^{\frac{n-1}{\alpha}} \qquad \textbf{5.4}$$

where η is the viscosity, $\eta_0$is the zero shear rate viscosity, η_∞ is the viscosity at the infinite shear rate, $1/\lambda$ is the critical shear rate for the onset of shear thinning, n-1 is the power law index and α represents the transition region between η_0 and the power law region.

5.2.3. Synthesis of starch-based macroinitiator (StBr)

Waxy potato starch (2.59 g, 16 mmol) and lithium chloride (1.02 g, 24 mmol) were added to a 250 mL three-necked flask (dried overnight at 100 ˚C before use) connected with a mechanical stirrer. The system was vacuumed under heat and backfilled with N_2 three times to remove residual water. Anhydrous DMAc (100 mL) was transferred to the flask and the mixture was stirred at 130 ˚C for about 1 h under N_2 atmosphere. A transparent solution formed when the mixture cooled down to room temperature naturally. The solution was cooled down with an ice bath and then 0.42 mL (4 mmol) BpB was added dropwise within 30 min under the protection of N_2. The mixture was then warmed up naturally to room temperature and stirred for 3 h. The final products were precipitated out with tenfold acetone and then filtered, washed and dried under vacuum at 45 ˚C for 24 h. The resulting white powder was then purified by Soxhlet extraction with acetone as the solvent for 24 h (final yield 87%).

5.2.4. Synthesis of starch-based copolymers by aqueous Cu^0-mediated LRP

Typical Polymerization Protocol. H_2O (100 mL), StBr (48.6 mg, 0.04 mmol), a mixture of AM and SAMPS (240 mmol in total) as well as Me_6TREN (23 μL, 0.08 mmol) were charged to a 250 mL three-neck round-bottom flask with a magnetic stirrer bar and rubber septum. The solution was deoxygenated by three freeze-pump-thaw cycles. Cu powder (5.2 mg, 0.08 mmol) was then added with rapid stirring under the protection of nitrogen. The mixture was allowed to react for 15 min at room temperature. The resulting solution was freeze-dried and followed by Soxhlet extraction with ethanol as the solvent for 48 h. The product was then vacuum dried at 65 ˚C for 48 h. For the purpose of short and clear, starch-g-poly(AM-co-SAMPS) was named in the following way: e.g. St-g-PSAMPS-P10, P10 stands for the mole ratio of SAMPS in the feeding AM/SAMPS monomer mixture is 10%. Starch-g-poly(AM-co-SAMPS-co-NIPAM) was named like St-g-PASAN-P25, P25 stands for the total mole percentage of SAMPS and NIPAM in the feeding AM/SAMPS/NIPAM monomer mixture is 25%.

5.2.5. Cleaving of graft polymer chains from the starch backbone

Starch-based graft polymer (0.25 g) was dissolved in 25 mL Milli-Q water in a round-bottom flask and then 0.25 mL concentrated hydrochloric acid was added. The mixture was stirred and refluxed at 100 ˚C for 3 h. The resulting free polymer was precipitated out with acetone, then filtered and washed with acetone for three times. The product was dried under vacuum at 60 ˚C for 24 h.

5.3. Results and discussion

The successful synthesis of water-soluble waxy potato starch-based macroinitiator (StBr) was proved by FT-IR and NMR (^{1}H-NMR, ^{13}C-NMR and gHSQC) characterization. Details could be seen in the supplementary materials (Figure S5-2 and Figure S5-3).

Compared with the synthesis of polymer with low degree of polymerization (DP), normally a higher catalyst/initiator ratio is needed to obtain high DP polymer with controlled Cu^0-mediated LRP. This is in agreement with literature [27]. As shown in Table 5-1, linear PSAMPS (co)polymers were synthesized with different DP (at different catalyst/initiator ratio) to verify the controllability of Cu^0-mediated LRP on the polymerization. PDI values in Table 5-1 suggest a relatively narrow distribution of (co)polymers which are proof of controlled polymerization.

Table 5-1. Experimental data of linear PSAMPS (co)polymer synthesized by Cu^0-mediated LRP

Sample	[M]:[L]:[Cu^0]:[L]	Monomer ratio [a]	Ratio (SAMPS)	DP [c]	PDI [d]
PSAMPS-DP50	50 : 1: 0.6: 0.6	100 : 0: 0	100	46	1.32
PSAMPS-DP500	500 : 1: 1: 0.8	100 : 0: 0	-	*N.A.*	-
PSAMPS-DP500	500 : 1: 2: 2	100 : 0: 0	100	390	1.47
PSAMPS-P25	2000 : 1: 2: 2	75 : 25: 0	23.5 [b]	1178	1.45

a. Ratio of AM: SAMPS: NIPAM in feeding solution; ***b.*** Composition of copolymer determined by elemental analysis, data see supplementary materials (Table S5-1); ***c.*** Degree of polymerization (DP) determined according to NMR and mass, *N.A.* means no reaction. ***d.*** Polydispersity index (PDI) determined by gel permeation chromatography (GPC).

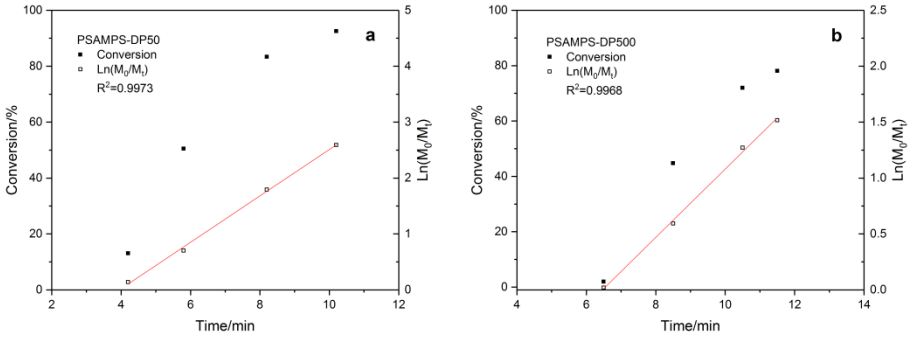

Figure 5-1. Kinetic plot of PSAMPS homopolymer synthesized by Cu^0-mediated LRP

For homopolymer the kinetic of polymerization was also monitored by ^{1}H-NMR and the kinetic plots (Figure 5-1) were thus obtained according to equation 5.5 [37].

$$\ln\left(M_0/M_t\right) = k_p\left(R_i/k_t\right)^{1/2}\cdot t \qquad \textbf{5.5}$$

where M_0 and M_t are the monomer concentration at the beginning of polymerization and at time t, respectively, k_p indicates the kinetic propagation constant, R_i the initiation rate while k_t the termination rate constant. Clearly, the linear relationship between ln(M_0/M_t) and t in Figure 5-1 reveals a controlled polymerization, which is in line with the PDI values from GPC (Table 5-1). Besides, the conversion and kinetic curves also indicate an induction period in polymerization which is attributed to the absence of soluble copper species (Cu^I and Cu^{II} species) at the beginning of polymerization [38].

A series of St-g-poly(AM-co-SAMPS-co-NIPAM) with different SAMPS and NIPAM molar intake was then synthesized by Cu^0-mediated LRP with StBr as initiator and copper powder/Me_6Tren as the catalyst system (see Table 5-2). Information for the synthesis of St-g-poly(AM-co-NIPAM) (St-g-PNIPAM-P10 and St-g-PNIPAM-P25, P10 and P25 stand for the molar ratio of NIPAM unit in the copolymer) is also listed in Table 5-2 for the clarity of discussion, details about these two copolymers are available in our previous report [12]. According to our previous work, the target DP for all the samples was set to 6000 to achieve satisfactory viscosity values for potential applications like EOR. The copolymers synthesized in the present work were characterized by FT-IR (Figure 5-2a) and ^{1}H-NMR (Figure 5-2b). The absorption peak around 3188 cm^{-1} in FT-IR spectrums was assigned to the stretch of N-H bond in the amide group. For the St-g-PSAMPS-P0, typical amide group peaks at 1652 cm^{-1} (amide I) and 1610 cm^{-1} (amide II) could also be seen in the spectrum. With the increasing of SAMPS and

(or) NIPAM intake in the copolymer, the amide I and II peaks gradually shifted to 1628 cm^{-1} and 1530 cm^{-1} respectively [39]. The symmetrical and asymmetrical stretch of S=O bond in the sulfonate group could also be seen at 1040 cm^{-1} and 1180 cm^{-1} respectively [40]. The ^{1}H-NMR spectra of the copolymers are shown in Figure 5-2b, in which the peak around 1.0 ppm was attributed to the methyl protons in the NIPAM unit (St-g-PASAN) while the peak around 1.3 ppm was attributed to the methyl protons in the SAMPS unit (St-g-PSAMPS). The peak at 3.8 ppm originates from the tertiary carbon protons in the NIPAM amide group while the broad peak in the range of 3.0 to 3.5 ppm originates from the SAMPS methine carbon (connected with the sulfonic group) protons. The signals in the range of 1.9 - 2.3 ppm and 1.2 - 1.8 ppm (partially overlap with the peak from SAMPS methyl protons) were assigned to the tertiary and secondary carbon protons in the copolymer backbone, respectively.

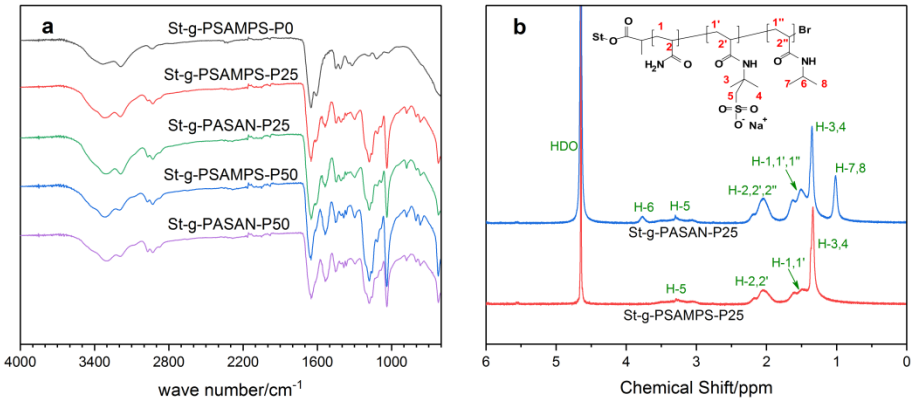

Figure 5-2. FT-IR (a) and ^{1}H-NMR (b) spectra of starch-based graft copolymers

As shown in Table 5-2, the mole ratio of SAMPS and NIPAM in the feeding monomer mixture were varied from 0% to 50% and 0% to 25% respectively while the overall target DP was set to 6000 for all the copolymers. Elemental analysis, instead of NMR due to the overlapping peaks in the spectra, was used to determine the mole percentage of SAMPS unit (for all copolymers) and AM unit (for copolymers with NIPAM) in the product according to equation 5.1 and 5.2 (see experiment part).

The polymerization kinetics were not monitored due to the relatively high rate and corresponding high solution viscosity. However, the controllability of Cu^{0}-mediated LRP on the grafting can be verified, although indirectly, by the PDI (obtained from GPC) of the (co)polymer cleaved from the starch backbone. As shown in Table 5-2, narrow molecular weight distribution (PDI < 1.6) which

suggests a reasonably controlled polymerization is observed after the hydrolyzation of the starch backbone. Similar to the GPC traces shown in other reports [41,42], the (co)polymers cleaved from the starch backbone also display a non-normal distribution (Figure S5-4). Given the rheological results shown below, copolymer with higher hydrodynamic volume (thus higher viscosity) displays larger deviation from normal distribution which might be explained by the residual "deactivation by propagation" as proposed in literature.[43]. Accordingly, although the "gel effect" at high conversion constrains the movement of polymer chains and thus results in the inefficient control on molecular weight, the activation/deactivation cycle can still be maintained because of the diffusion of activation/deactivation species. Moreover, the radical centers can also "reach" the deactivation species by propagation (residual deactivation) which is helpful to lower the PDI.

Table 5-2. Experimental data of starch-based grafted copolymer synthesized by Cu^0-mediated LRP

Sample	Monomer ratio [a]	Time /min	Conversion/% [b]			Ratio [c]		DP [b]	PDI [d]
			AM	AMPS	NIPAM	AMPS	NIPAM		
St-g-PSAMPS-P0	100 : 0: 0	12	91.56	-	-	-	-	5554	1.42
St-g-PSAMPS-P10	90 : 10: 0	12	96.95	94.80	-	9.8	-	5804	1.47
St-g-PNIPAM-P10	90 : 0: 10	12	80.66	-	80.66	-	10.0	4840	1.64
St-g-PSAMPS-P25	75 : 25: 0	15	90.67	90.19	-	24.9	-	5433	1.51
St-g-PNIPAM-P25	75 : 0: 25	15	92.57	-	82.95	-	23.0	5410	- [e]
St-g-PASAN-P25	75 : 15: 10	15	89.55	90.26	91.96	15.1	10.2	5394	1.54
St-g-PASAN-P50	50 : 25: 25	20	86.19	85.26	95.34	24.2	27.0	5295	- [e]
St-g-PSAMPS-P50	50 : 50: 0	18	92.25	83.80	-	47.6	-	5282	1.53

a. Ratio of AM: SAMPS: NIPAM. Overall ratio for the grafting [M]: [I]: [Cu^0]: [L]= 6000: 1: 2: 2; ***b.*** Monomer conversion and polymer degree of polymerization (DP) determined by elemental analysis (or NMR) and mass; ***c.*** Composition of grafted chains determined according to elemental analysis or NMR; ***d.*** Polydispersity index (PDI) of copolymer after the hydrolyzation of starch backbone; ***e.*** Not available due to the potential high intermolecular association, leading to retention of the polymer inside the GPC column

To investigate the influence of chain composition on copolymer solution properties, a series of rheological tests were carried out. For a polymer with a given molecular structure, the intrinsic viscosity is an indication of the hydrodynamic volume of polymers [44,45]. The intrinsic viscosity can be obtained by extrapolating

the plot of ln(η_{red}) against polymer concentration to c = 0 (see Experimental section). It should be noted that for linear polyelectrolytes the electrostatic repulsion expands the macromolecule coil in dilute solution due to intramolecular repulsion but compress that in higher concentration because of intermolecular repulsion. As a result, higher reduced viscosity can be observed at lower polymer concentration (known as polyelectrolyte effect). This makes the extrapolation to infinite dilution quite unreliable, so the measurements for linear polyelectrolyte usually are carried out in salt solution (like 0.1 M NaCl) to screen out the influence of charges [46,47]. However, this makes the comparison between samples inconvenient as the salt concentration varies in order to effectively shield different charge density while the final result is also related to the salt concentration [48]. Furthermore, in the case of highly branched polyelectrolytes, the steric hindrance and strong intramolecular Coulomb repulsion may, to some extent, offset the "polyelectrolyte effect" encountered by linear ones. This makes the measurement and comparison of intrinsic viscosity in salt-free solution possible. Attempts were made with Martin equation in the present research and results are shown in Figure 5-3 (part of the data for ln(η_{red}) vs concentration were shown in Figure S5-5 for clarity).

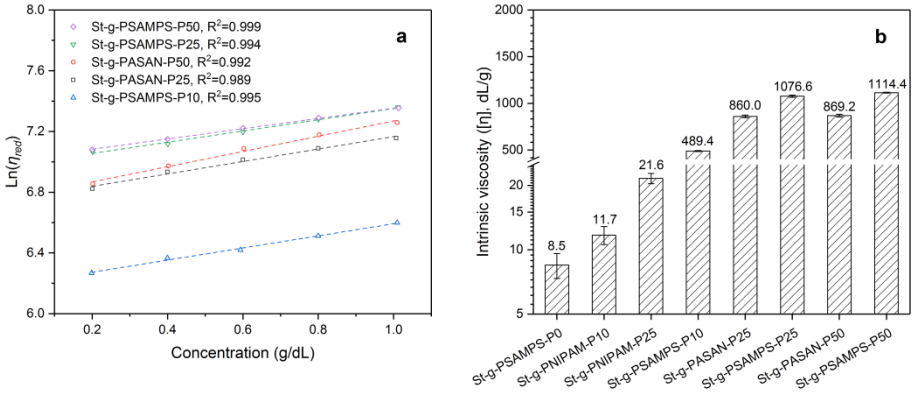

Figure 5-3. Reduced viscosity as a function of polymer concentration (Martin equation) (a) and corresponding intrinsic viscosity (b)

As can be observed in Figure 5-3b, with the same molar ratio in the copolymer, SAMPS unit can expand the hydrodynamic volume of the grafted copolymer more significantly than the NIPAM unit due to the Coulomb repulsion forces. The changes in the intrinsic viscosity between grafted AM/SAMPS copolymers (St-g-PSAMPS) also signify an optimum SAMPS intake (25 mol%) in the composition. Interestingly, compared to the increase of intrinsic viscosity between St-g-PASAN-

P25 (15 mol% SAMPS and 10 mol% NIPAM) and St-g-PSAMPS-P10 (10 mol% SAMPS), a decrease can be observed between St-g-PSAMPS-P25 (25 mol% SAMPS) and St-g-PASAN-P50 (25 mol% SAMPS and 25 mol% NIPAM), indicates a negative influence of NIPAM unit on the hydrodynamic volume of the copolymer. This trend is in agreement with the sequence of copolymers' low shear rate viscosity (γ < 10 s^{-1} in Figure 5-4a) which is more related with the hydrodynamic volume and excluded volume [49-51]. One may argue that the (co)polymer concentration is still too high to show the "polyelectrolyte effect". However, this effect can be observed in the same concentration range according to one previous report on spherical polyelectrolytes [52]. Nevertheless, the validity of measuring the intrinsic viscosity of synthesized starch-based branched polyelectrolytes with the Martin equation in salt-free water still needs further investigation.

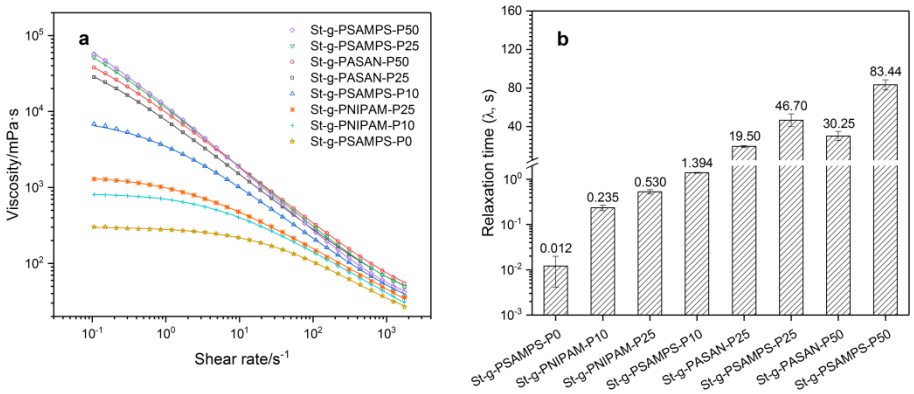

Figure 5-4. Viscosity as a function of shear rate (a, 1.2 *wt.*% copolymer solution) and corresponding relaxation time from Carreau-Yasuda model (b)

The influence of chain composition on solution viscosity as a function of shear rate was also evaluated at the same polymer concentration, the result of which is shown in Figure 5-4a. It is clear that, due to the extended macromolecular chains resulting from the electrostatic repulsion, the viscosity of AM/SAMPS copolymers (St-g-PSAMPS) is much higher than that of AM/NIPAM copolymers (St-g-PNIPAM), especially in the low shear rate region. It is also noticed that copolymers with higher SAMPS intake (e.g. > 25 mol%, St-g-PSAMPS-P50) are more shear sensitive at a high shear rate (> 10 s^{-1}) than other copolymers. This is attributed to the weak inter-chain entanglement because of the electrostatic repulsion. Furthermore, these data were also fitted with the Carreau-Yasuda model (see Experimental section) to study the influence of chain composition on the copolymer relaxation time (λ) [9,35,36]. As indicated in Figure 5-4b, a higher SAMPS

intake results in higher λ values, thus, the lower critical shear thinning rate (1/λ) should be observed in the flow curve. This is in line with Figure 5-4a which shows a shift in the onset of shear thinning behavior towards lower shear rate regions. In the case of AM/SAMPS/NIPAM copolymer, high NIPAM intake, like its effect on the intrinsic viscosity, reduces the relaxation time which means the copolymer solution is less shear sensitive (see the λ of St-g-PSAMPS-P25, St-g-PASAN-P50 and corresponding flow curve in Figure 5-4). This may be related to the intermolecular association because of the high ratio of NIPAM units.

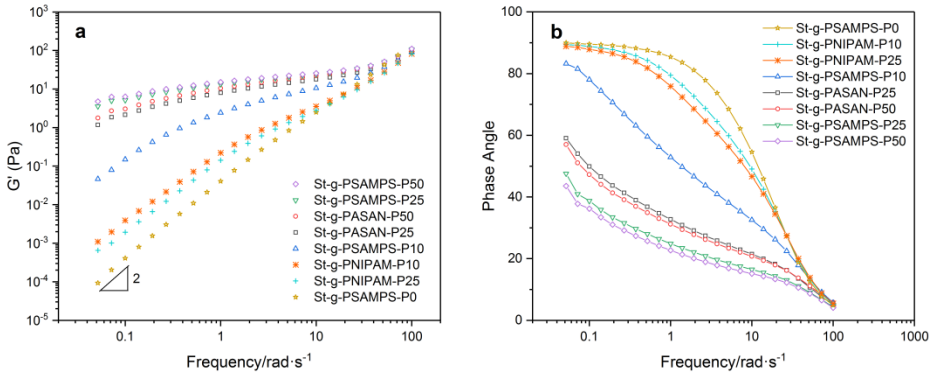

Figure 5-5. The storage (G') (a) and phase angle (b) as a function of frequency at 1.2 *wt.*% polymer concentration

Besides viscosity, the viscoelastic property also affects the performance of polymers in applications like improving the sweep efficiency in EOR[53]. The influence of composition on the viscoelastic properties of the copolymers is shown in Figure 5-5 (for clarity the plot of loss modulus vs. frequency is shown in Figure S5-6). In Figure 5-5a, in the terminal zone (low frequency region), typical Maxwell flow behavior with G' proportional to ω^2 (slope = 2) and G" directly proportional to the angular frequency (ω) (slope = 1) can be observed for samples with no (or low) SAMPS intake [54]. For copolymers with high SAMPS intake (e.g. > 15 mol%, St-g-PASAN-P25), deviation in the slope from the Maxwell model is observed which suggests intermolecular entanglement [49]. Like the viscosity profile shown in the flow curve in Figure 5-4a, both the storage modulus (G') and the loss modulus (G'') of SAMPS copolymers (St-g-PSAMPS and St-g-PASAN) increased more significantly (ω < 20 rad/s) compared with those of St-g-PNIPAM. The same trend can also be observed in the change of solution elastic response as indicated by the phase angles at equal copolymer concentration. All these results, like the intrinsic viscosity and viscosity vs shear rate curve (vide supra), indicate an optimum SAMPS ratio (25 mol%) in the AM/SAMPS copolymers as well.

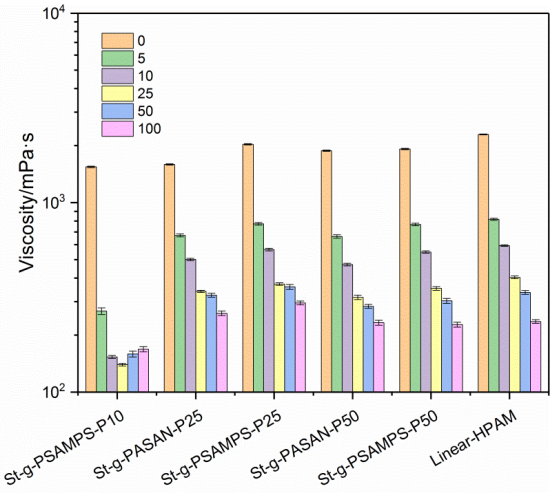

Figure 5-6. Viscosity (γ = 10 s^{-1}) as a function of salinity (unit in kilo ppm) for starch-based graft copolymers (1.0 *wt.*%)

As evidenced by the results shown above, at high molar ratio the NIPAM intake displays a negative influence on the rheological performance of SAMPS copolymer in fresh water. In application areas like EOR, inorganic electrolyte presents in the solution can screen the Coulomb forces which may result in different rheology behavior. Thus, the influence of salt and NIPAM intake on the viscosity of copolymer was also studied in saline water with different NaCl concentration. As shown in Figure 5-6, all the SAMPS copolymers display higher viscosity than that of AM/NIPAM copolymers (optimally, 220 mP·s of St-g-PNIPAM-P25, see Chapter 4) when the SAMPS intake is high enough (e.g. > 10 mol%). Comparison between different St-g-SAMPS copolymers also indicates 25% is the optimum SAMPS ratio for their saline resistance in viscosity: while lower ratio is not enough to effectively break down the intramolecular hydrogen bond between AM units in saline water (St-g-PSAMPS10), higher ratio makes the hydrodynamic volume of the copolymers more sensitive to salt (St-g-PSAMPS50). In the case of St-g-PASAN, the incorporation of NIPAM unit leads to a lower viscosity which is related to the stronger association of NIPAM units at high salt concentration due to the collapse of macromolecule (see the viscosity of St-g-PSAMPS-P25 and St-g-PASAN-P50 in Figure 5-6). This negative effect of NIPAM can also be observed when comparing the viscosity of St-g-PASAN-P25 (15 mol% SAMPS and 10 mol% NIPAM) and St-g-PASAN-P50 (25 mol% SAMPS and 25 mol% NIPAM). Although St-g-PASAN-P50 displays higher viscosity than St-g-PASAN-P25 in pure water, a lower viscosity is observed in saline water.

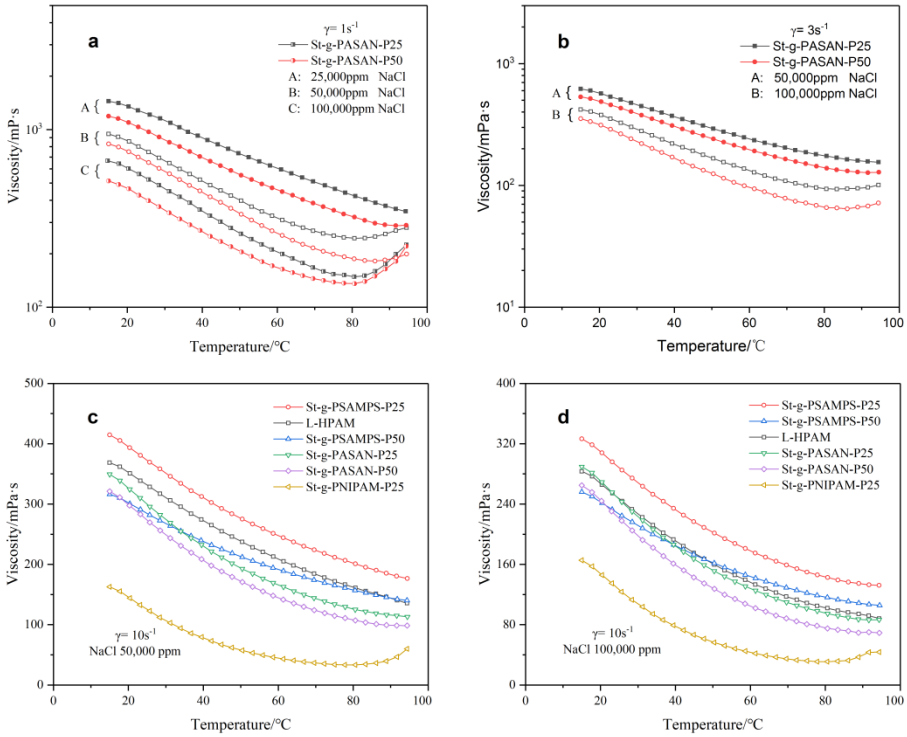

Figure 5-7. Viscosity versus temperature of waxy potato starch-based AM/SAMPS/NIPAM copolymers in saline water at different shear rate (1.0 *wt.*% copolymer concentration)

Besides the influence of NIPAM on the room temperature rheology, the thermo-thickening behavior of NIPAM copolymer is also of interest for applications like EOR. According to our previous report, the thermo-thickening behavior is not only affected by the intake of NIPAM unit, but also by the strong intramolecular hydrogen bond in waxy starch-based highly branched acrylamide copolymer [12]. In the present research, the Coulomb repulsion between SAMPS units breaks down the intramolecular hydrogen bond and also hinder the intermolecular association of NIPAM units in fresh and low salinity (< 25000 ppm) water. As a result, no thermo-thickening behavior is observed at the shear rate of $1s^{-1}$ in group A of Figure 5-7a. With the increasing salinity, charges on the polymer chains are screened effectively which makes the hydrophobic association of NIPAM units possible. This is proved by the thermo-thickening behavior indicated by group B (Figure 5-7a) and the more obvious increment of viscosity in higher salinity solution (Figure 5-7a, group C). At higher shear rate (γ = 3 s^{-1}) the hydrophobic association can be disrupted, as the result of which thermo-thickening is only

observed at really high salinity (more hydrophobic association) as can be seen in Figure 5-7b. At an even higher shear rate, for example the average shear rate in porous media (γ = 10 s^{-1}) as reported, no thermo-thickening behavior of St-g-PASAN is observed in Figure 5-7c and Figure 5-7d [55,56]. The viscosity-temperature profiles of different copolymers are also shown in the same graph for comparison. As can be observed (Figure 5-6 and Figure 5-7d), although the linear partially hydrolyzed polyacrylamide (L-HPAM) has a higher viscosity (2290 mPa·s) in freshwater than that of the starch-based copolymers (highest 2032 mPa·s), St-g-PSAMPS copolymers display better temperature and saline resistance due to the branched structure. This is more obvious in the case of St-g-PSAMPS-P50 which has a lower viscosity under room temperature compared with other copolymers but displays higher viscosity than L-HPAM and St-g-PASAN copolymers at high temperature and salinity. This may also be related to its higher charge density in comparison with other copolymers. Considering the higher viscosity of St-g-PASAN-P50 relative to that of St-g-PASAN-P25 in fresh water (Figure 5-6), the intake of high mole ratio of NIPAM unit in the copolymer again proved to play a negative role on the saline resistance property of copolymer in a wide temperature range.

5.4. Conclusions

In this work, a water-soluble macroinitiator was synthesized by homogeneous esterification of waxy potato starch with 2-bromopropionyl bromide in *N*,*N*-dimethylacetamide (DMAc). Based on this, a series of branched random copolymers of acrylamide (AM), sodium 2-acrylamido-2-methyl-1-propanesulfonate (SAMPS) and *N*-isopropylacrylamide (NIPAM) were prepared by aqueous Cu^0-mediated living radical polymerization (Cu^0-mediated LRP) at room temperature. The mole ratios of SAMPS and NIPAM were varied in the range of 0% - 50% and 0% - 25% respectively to investigate the influence of chain composition on aqueous rheological properties of copolymers as well as their thermo-responsive properties. Due to the negatively charged side groups, waxy potato starch-based AM/SAMPS copolymers (St-g-PSAMPS) displayed much higher viscosity than AM/NIPAM copolymers (St-g-PNIPAM) in saline solution. Comparison of intrinsic viscosity, viscosity profile at different shear rates and salinity between different St-g-PSAMPS copolymers indicated an optimum SAMPS ratio (25 mol%) for the balanced performance of viscosity and salt resistance. The intake of a high ratio of NIPAM unit undermines the thickening ability of tricomponent copolymers (St-g-PASAN) in both fresh and saline water due to the hydrophobic association. In high salinity solution, the hydrodynamic volume of the macromolecule collapses due to the screening effect of salt on the

charged SAMPS units. As the result, thermo-thickening behavior can be observed at low shear rates ($\gamma \leqslant 3\ s^{-1}$) because of hydrophobic association. At a higher shear rate, the thermo-thickening behavior disappears due to the disruption of association.

5.5. Acknowledgements

This work was performed under the financial support from the China Scholarship Council (CSC) with Grant Number 201406380107. We thank Avebe (Veendam, The Netherlands) for the donation of the waxy potato starch.

5.6. References

1 Romero-Zerón, L. in *Introduction to enhanced oil recovery (EOR) Processes and Bioremediation of Oil-Contaminated Sites* Ch. 1, (InTech, 2012).
2 Wei, B., Romero-Zerón, L. & Rodrigue, D. Oil displacement mechanisms of viscoelastic polymers in enhanced oil recovery (EOR): a review. *Journal of Petroleum Exploration and Production Technology* **4**, 113-121, (2013).
3 IEA. Key World Energy Statistics. (2015).
4 Hashmet, M. R., AlSumaiti, A. M., Qaiser, Y. & S. AlAmeri, W. Laboratory investigation and simulation modeling of polymer flooding in high-temperature, high-salinity carbonate reservoirs. *Energy & Fuels* **31**, 13454-13465, (2017).
5 Ge, J. & Wang, Y. Surfactant enhanced oil recovery in a high temperature and high salinity carbonate reservoir. *Journal of Surfactants and Detergents* **18**, 1043-1050, (2015).
6 Strand, S., Puntervold, T. & Austad, T. Effect of temperature on enhanced oil recovery from mixed-wet chalk cores by spontaneous imbibition and forced displacement using seawater. *Energy & Fuels* **22**, 3222-3225, (2008).
7 Zheng, J. *et al.* Offshore produced water management: A review of current practice and challenges in harsh/Arctic environments. *Marine Pollution Bulletin* **104**, 7-19, (2016).
8 Robinson, D. Oil and gas: Treatment of produced waters for injection and reinjection. *Filtration + Separation* **50**, 36-43, (2013).
9 Wever, D. A. Z., Polgar, L. M., Stuart, M. C. A., Picchioni, F. & Broekhuis, A. A. Polymer molecular architecture as a tool for controlling the rheological properties of aqueous polyacrylamide solutions for enhanced oil recovery. *Industrial & Engineering Chemistry Research* **52**, 16993-17005, (2013).
10 Wever, D. A. Z., Picchioni, F. & Broekhuis, A. A. Branched polyacrylamides: Synthesis and effect of molecular architecture on solution rheology. *European Polymer Journal* **49**, 3289-3301, (2013).
11 Wever, D. A. Z., Riemsma, E., Picchioni, F. & Broekhuis, A. A. Comb-like thermoresponsive polymeric materials: Synthesis and effect of

macromolecular structure on solution properties. *Polymer* **54**, 5456-5466, (2013).
12 Fan, Y., Boulif, N. & Picchioni, F. Thermo-responsive starch-g-(PAM-co-PNIPAM): Controlled synthesis and effect of molecular components on solution rheology. *Polymers* **10**, 92, (2018).
13 Zobel, H. F. Molecules to Granules: A comprehensive starch review. *Starch - Stärke* **40**, 44-50, (1988).
14 Jane, J.-l. in *Chemical and functional properties of food saccharides* (ed Piotr Tomasik) (CRC Press, 2004).
15 Yoo, S.-H. & Jane, J.-l. Molecular weights and gyration radii of amylopectins determined by high-performance size-exclusion chromatography equipped with multi-angle laser-light scattering and refractive index detectors. *Carbohydrate Polymers* **49**, 307-314, (2002).
16 Li, X. e., Xu, Z., Yin, H., Feng, Y. & Quan, H. Comparative studies on enhanced oil recovery: Thermoviscosifying polymer versus polyacrylamide. *Energy & Fuels* **31**, 2479-2487, (2017).
17 Seright, R. S., Campbell, A., Mozley, P. & Han, P. Stability of partially hydrolyzed polyacrylamides at elevated temperatures in the absence of divalent cations. *SPE Journal* **15**, 341-348, (2010).
18 Wang, F., Jeon, J.-H., Kim, S.-J., Park, J.-O. & Park, S. An eco-friendly ultra-high performance ionic artificial muscle based on poly(2-acrylamido-2-methyl-1-propanesulfonic acid) and carboxylated bacterial cellulose. *Journal of Materials Chemistry B* **4**, 5015-5024, (2016).
19 Zhao, P. *et al.* Polyelectrolyte-promoted forward osmosis process for dye wastewater treatment – Exploring the feasibility of using polyacrylamide as draw solute. *Chemical Engineering Journal* **264**, 32-38, (2015).
20 Ge, Q., Wang, P., Wan, C. & Chung, T. S. Polyelectrolyte-promoted forward osmosis-membrane distillation (FO-MD) hybrid process for dye wastewater treatment. *Environmental Science & Technology* **46**, 6236-6243, (2012).
21 Sahiner, N. & Seven, F. Energy and environmental usage of super porous poly(2-acrylamido-2-methyl-1-propan sulfonic acid) cryogel support. *RSC Advances* **4**, 23886-23897, (2014).
22 Qi, L., Wanfen, P., Yabo, W. & Tianhong, Z. Synthesis and assessment of a novel AM-co-AMPS polymer for enhanced oil recovery (EOR). 997-1000, (2013).
23 Song, H., Zhang, S.-F., Ma, X.-C., Wang, D.-Z. & Yang, J.-Z. Synthesis and application of starch-graft-poly(AM-co-AMPS) by using a complex initiation system of CS-APS. *Carbohydrate Polymers* **69**, 189-195, (2007).
24 Lee, J. *et al.* Behavior of spherical poly(2-acrylamido-2-methylpropanesulfonate) polyelectrolyte brushes on silica nanoparticles up to extreme salinity with weak divalent cation binding at ambient and high temperature. *Macromolecules* **50**, 7699-7711, (2017).
25 Cheng, Y. *et al.* Water-dispersible reactive nanosilica and poly(2-acrylamido-

2-methyl-1-propanesulfonic acid sodium) nanohybrid as potential oil displacement agent for enhanced oil recovery. *Energy & Fuels* **31**, 6345-6351, (2017).

26 Zou, W. *et al.* Synthesis and characterization of biodegradable starch-polyacrylamide graft copolymers using starches with different microstructures. *Journal of Polymers and the Environment* **21**, 359-365, (2012).

27 Jones, G. R. *et al.* Rapid synthesis of well-defined polyacrylamide by aqueous Cu(0)-mediated reversible-deactivation radical polymerization. *Macromolecules* **49**, 483-489, (2016).

28 Masci, G., Giacomelli, L. & Crescenzi, V. Atom transfer radical polymerization of sodium2-acrylamido-2-methylpropanesulfonate. *Journal of Polymer Science Part A: Polymer Chemistry* **43**, 4446-4454, (2005).

29 McCullough, L. A., Dufour, B. & Matyjaszewski, K. Incorporation of poly(2-acrylamido-2-methyl-*N*-propanesulfonic acid) segments into block and brush copolymers by ATRP. *Journal of Polymer Science Part A: Polymer Chemistry* **47**, 5386-5396, (2009).

30 Nikolaou, V. *et al.* Polymerisation of 2-acrylamido-2-methylpropane sulfonic acid sodium salt (NaAMPS) and acryloyl phosphatidylcholine (APC) via aqueous Cu(0)-mediated radical polymerisation. *Polymer Chemistry* **7**, 2452-2456, (2016).

31 Zhang, C. *et al.* Dissolution mechanism of cellulose in *N,N*-dimethylacetamide/lithium chloride: revisiting through molecular interactions. *Journal of Physical Chemistry B* **118**, 9507-9514, (2014).

32 El Seoud, O. A., Nawaz, H. & Areas, E. P. Chemistry and applications of polysaccharide solutions in strong electrolytes/dipolar aprotic solvents: an overview. *Molecules* **18**, 1270-1313, (2013).

33 Roland N. Icke, B. B. W., and Gordon A. Alles. β-Phenylethyldimethylamine. *Organic Syntheses* **25**, 89-92, (1945).

34 Masuelli, M. A. & Sansone, M. G. in *Products and applications of biopolymers* (InTech, 2012).

35 Yasuda, K., Armstrong, R. & Cohen, R. Shear flow properties of concentrated solutions of linear and star-branched polystyrenes. *Rheologica Acta* **20**, 163-178, (1981).

36 Carreau, P. J. Rheological equations from molecular network theories. *Transactions of the Society of Rheology* **16**, 99-127, (1972).

37 Goto, A. & Fukuda, T. Kinetics of living radical polymerization. *Progress in Polymer Science* **29**, 329-385, (2004).

38 Gao, Y., Zhao, T., Zhou, D., Greiser, U. & Wang, W. Insights into relevant mechanistic aspects about the induction period of Cu^0/Me_6TREN-mediated reversible-deactivation radical polymerization. *Chemical Communications* **51**, 14435-14438, (2015).

39 Beattie, D. A., Addai-Mensah, J., Beaussart, A., Franks, G. V. & Yeap, K. Y. In situ particle film ATR FTIR spectroscopy of poly (*N*-isopropyl acrylamide)

(PNIPAM) adsorption onto talc. *Physical Chemistry Chemical Physics* **16**, 25143-25151, (2014).
40 Zhu, J. *et al.* Surface zwitterionic functionalized graphene oxide for a novel loose nanofiltration membrane. *Journal of Materials Chemistry A* **4**, 1980-1990, (2016).
41 Achilleos, M., Demetriou, M., Marinica, O., Vekas, L. & Krasia-Christoforou, T. An innovative synthesis approach toward the preparation of structurally defined multiresponsive polymer (co)networks. *Polymer Chemistry* **5**, 4365, (2014).
42 Li, H., Miao, H., Gao, Y., Li, H. & Chen, D. Efficient synthesis of narrowly dispersed amphiphilic double-brush copolymers through the polymerization reaction of macromonomer micelle emulsifiers at the oil-water interface. *Polymer Chemistry* **7**, 4476-4485, (2016).
43 Rabea, A. & Zhu, S. Modeling the influence of diffusion-controlled reactions and residual termination and deactivation on the rate and control of bulk ATRP at high conversions. *Polymers* **7**, 819-835, (2015).
44 Arvidson, S. A., Rinehart, B. T. & Gadala-Maria, F. Concentration regimes of solutions of levan polysaccharide from Bacillus sp. *Carbohydrate Polymers* **65**, 144-149, (2006).
45 Lee, J. & Tripathi, A. Intrinsic viscosity of polymers and biopolymers measured by microchip. *Analytical Chemistry* **77**, 7137-7147, (2005).
46 Kulicke, W.-M. & Clasen, C. *Viscosimetry of polymers and polyelectrolytes*. (Springer Science & Business Media, 2013).
47 Badiger, M. V., Gupta, N. R., Eckelt, J. & Wolf, B. A. Intrinsic viscosity of aqueous solutions of carboxymethyl guar in the presence and in the absence of salt. *Macromolecular Chemistry and Physics* **209**, 2087-2093, (2008).
48 Xiong, X. & Wolf, B. A. Intrinsic viscosities of polyelectrolytes: specific salt effects and viscometric master curves. *Soft Matter* **10**, 2124-2131, (2014).
49 Gupta, R. K. *Polymer and composite rheology*. (CRC Press, 2000).
50 Macosko, C. W. *Rheology: principles, measurements, and applications*. (Wiley-vch, 1994).
51 Shawki, S. & Hamielec, A. The effect of shear rate on the molecular weight determination of acrylamide polymers from intrinsic viscosity measurements. *Journal of Applied Polymer Science* **23**, 3323-3339, (1979).
52 Antonietti, M., Briel, A. & Förster, S. Intrinsic viscosity of small spherical polyelectrolytes: Proof for the intermolecular origin of the polyelectrolyte effect. *The Journal of chemical physics* **105**, 7795-7807, (1996).
53 Zhu, D., Zhang, J., Han, Y., Wang, H. & Feng, Y. Laboratory study on the potential EOR use of HPAM/VES hybrid in high-temperature and high-salinity oil reservoirs. *Journal of Chemistry* **2013**, 1-8, (2013).
54 Picout, D. R. & Ross-Murphy, S. B. *Thermoreversible and irreversible physical gels from biopolymers*. (Marcel Dekker, Inc.: New York, 2002).
55 Berg, S. & van Wunnik, J. Shear rate determination from pore-scale flow

fields. *Transport in Porous Media* **117**, 229-246, (2017).
56 Niu, Y. *et al.* in *SPE International Symposium on Oilfield Chemistry* (Society of Petroleum Engineers, Houston, Texas, 2001).

5.7. Supplementary materials

The synthesis of starch-based macroinitiator

The starch-based macroinitiator StBr was prepared homogeneously via one step esterification reaction with 2-bromopropionyl bromide (BpB) in DMAc/LiCl as depicted in Scheme S5-1. Both FT-IR (Figure S5-2) and NMR (Figure S5-3 a ^{1}H-NMR, b ^{13}C-NMR, c gHSQC) were employed to demonstrate the successful preparation of the macroinitiator. The absorption peak at 1743 cm^{-1} in FT-IR spectrum was assigned to the stretch of the C=O group from the initiator while the peak at 1281 cm^{-1} was attributed to the C-O bond in the ester group. The successful synthesis of StBr was further proved by NMR spectra. In Figure S5-3a, the peak at 5.4 ppm should be assigned to the proton attached to the anomeric carbon and peaks in the range of 3.3 - 4.2 ppm should be attributed to the rest protons of the anhydroglucose unit (AGU). Peaks around 1.7 ppm and 4.7 ppm belong to methyl protons and methine proton of the 2-bromopropionyl group, respectively. The degree of esterification (DS) of StBr could be quantified with the peak at 5.4 ppm and 4.7 ppm. In the ^{13}C NMR spectrum (Figure S5-3b), the peak at 100 ppm belongs to the anomeric carbon and the peaks range from 60 ppm to 80 ppm should be assigned to the rest AGU carbons. The resonance of methyl and methine carbon locate at 22 ppm and 54 ppm respectively. These assignments are verified by the gHSQC spectrum (Figure S5-3c).

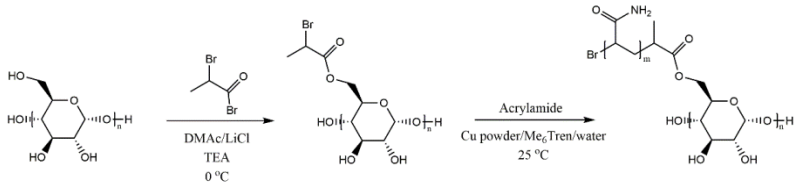

Scheme S5-1. Synthesis of waxy potato starch-based macroinitiator and St-g-PAM

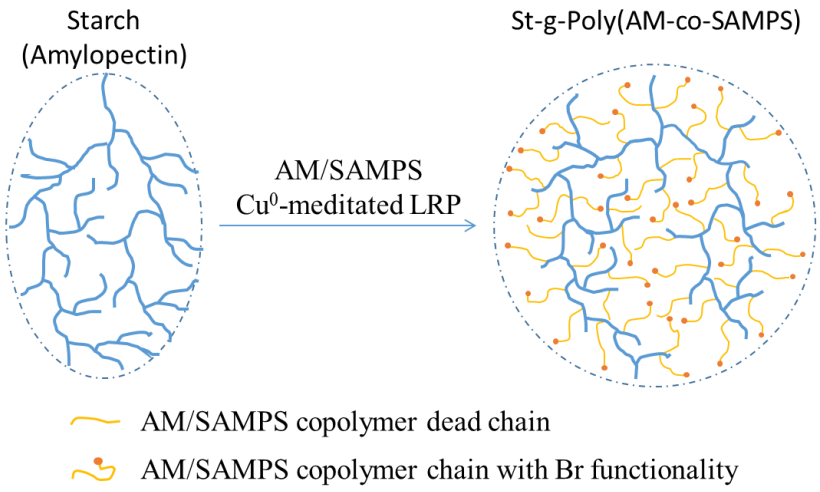

Figure S5-1. Illustration for the highly branched structure of amylopectin and its copolymer

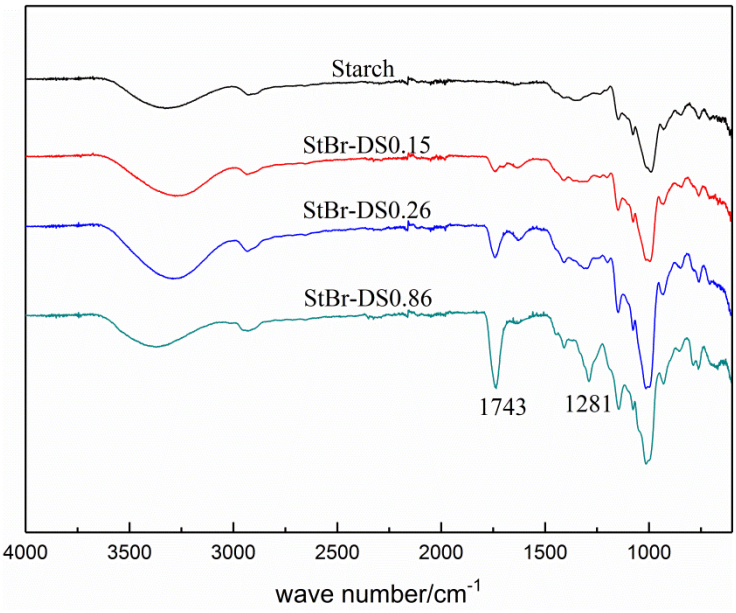

Figure S5-2. FT-IR spectra of StBr with different DS

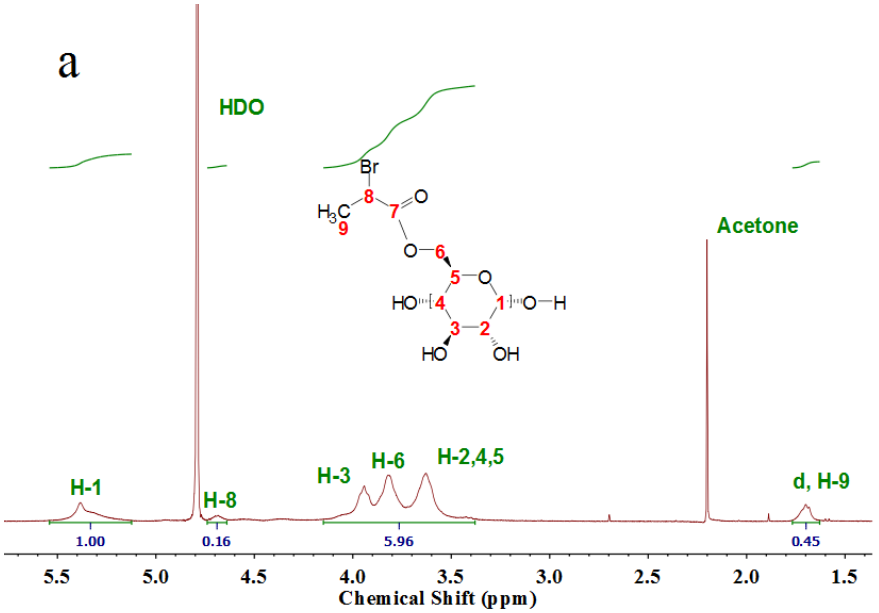
a
HDO
Acetone
H-1
H-8
H-3
H-6
H-2,4,5
d, H-9
1.00
0.16
5.96
0.45
5.5
5.0
4.5
4.0
3.5
3.0
2.5
2.0
1.5
Chemical Shift (ppm)

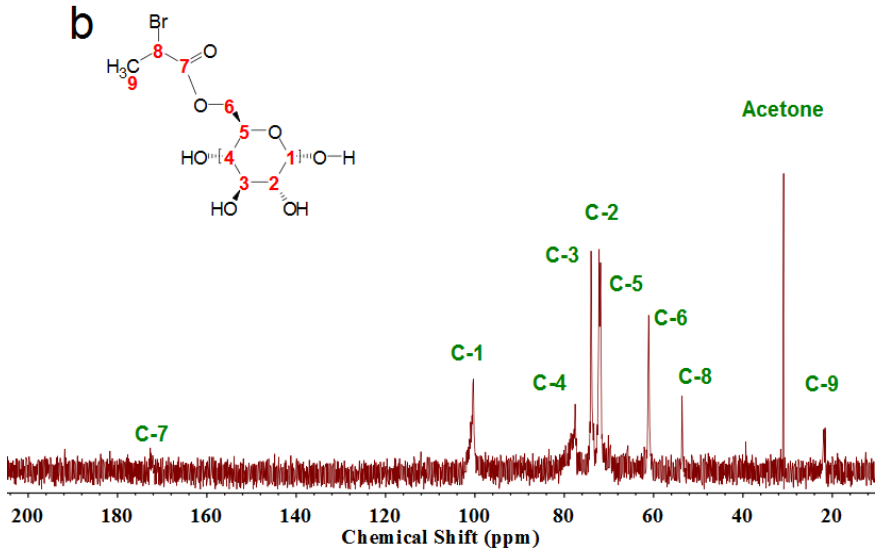
b
Acetone
C-1
C-2
C-3
C-4
C-5
C-6
C-7
C-8
C-9
200
180
160
140
120
100
80
60
40
20
Chemical Shift (ppm)

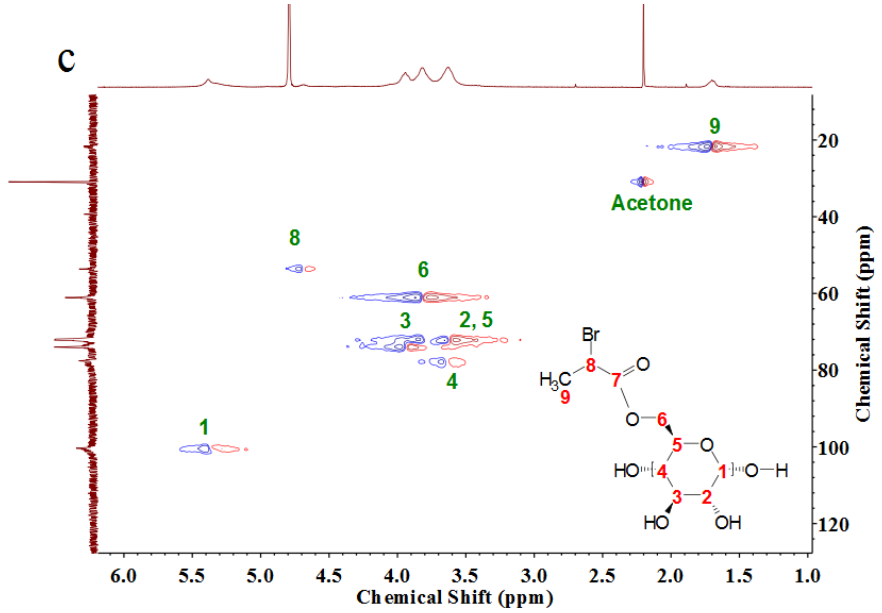

Figure S5-3. ^{1}H-NMR (a), ^{13}C-NMR (b) and gHSQC (c) spectra of StBr (DS = 0.15) in D_2O

Table S5-1. Elemental analysis result of the starch-based graft copolymer

Sample	C/% [a]	N/%	S/%	H/% [a]
PSAMPS-P25		11.80	6.31	
		11.62	6.29	
St-PSAMPS-P10	-	14.07	3.15	-
	-	14.00	3.14	-
St-PSAMPS-P25	-	11.21	6.4	-
	-	11.22	6.37	-
St-PSAMPS-P50	-	8.56	9.54	-
	-	8.50	9.02	-
St-PASAN-P25	43.03	12.82	4.49	7.01
	43.59	13.03	4.41	7.06
St-PASAN-P50	42.45	10.38	5.73	7.24
	42.83	10.45	5.77	7.29

a. - not accurate due to the residual ethanol, no further purification is needed as no influence on the result

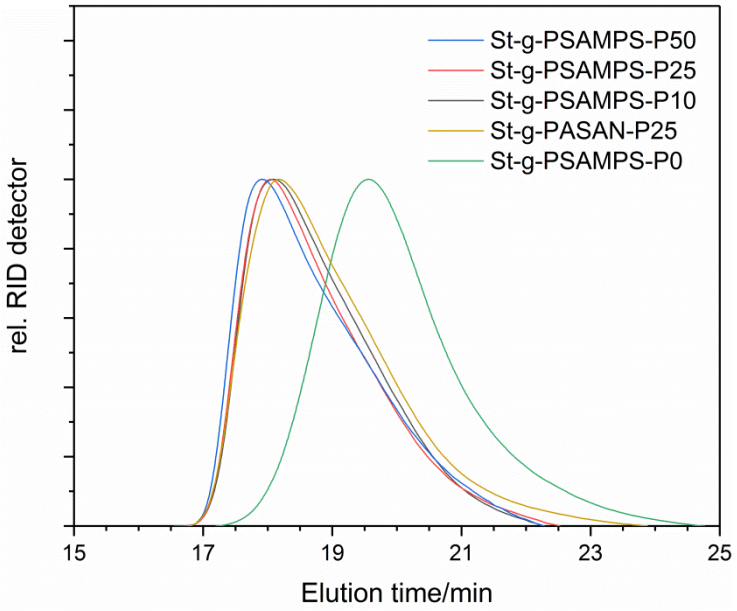

Figure S5-4. GPC traces of (co)polymers cleaved from the starch backbone

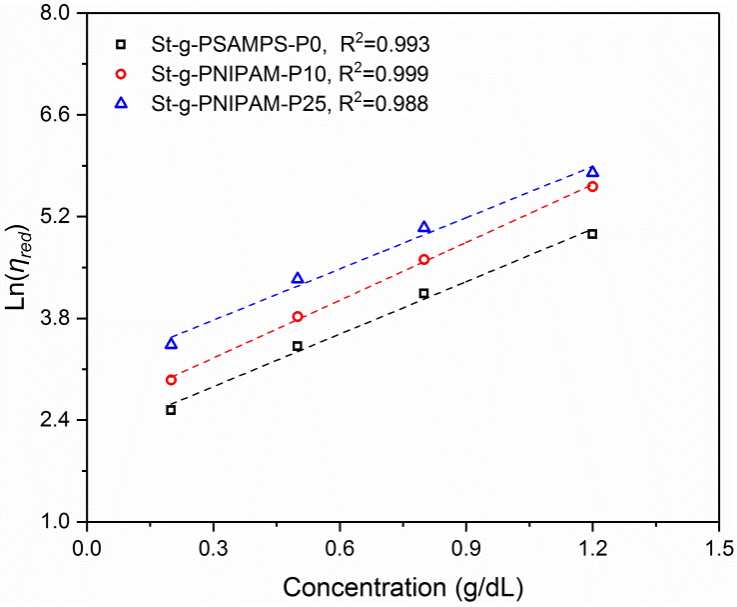

Figure S5-5. Reduced viscosity as a function of polymer concentration (Martin equation)

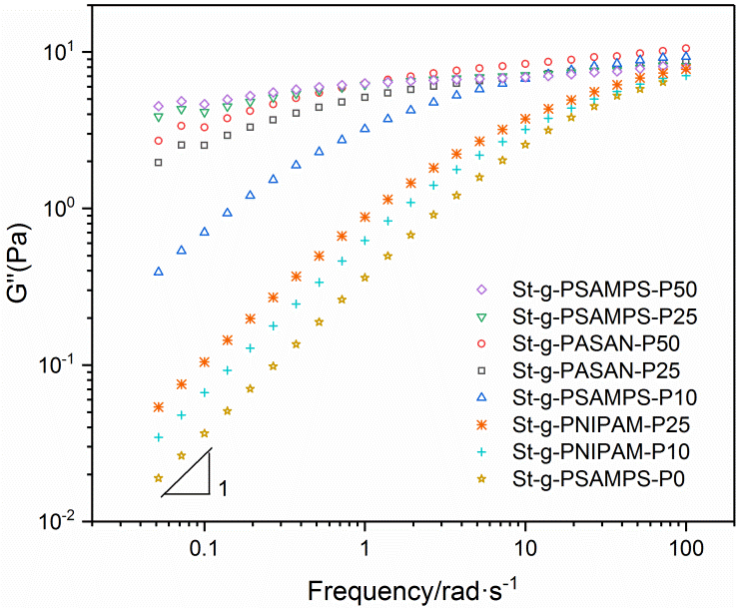

Figure S5-6. Loss modulus vs. frequency of starch-based copolymer (1.2 *wt.*%)